J Neurophysiol 94: 1048–1056, 2005.
First published April 20, 2005; doi:10.1152/jn.01276.2004.

Quantal Encoding of Information in a Retinal Ganglion Cell

Michael A. Freed
Department of Neuroscience, University of Pennsylvania School of Medicine, Philadelphia, Pennsylvania

Submitted 13 December 2004; accepted in final form 14 April 2005

Freed, Michael A. Quantal encoding of information in a retinal ganglion cell. *J Neurophysiol* 94: 1048–1056, 2005. First published April 20, 2005; doi:10.1152/jn.01276.2004. A retinal ganglion cell receives information about a white-noise stimulus as a flickering pattern of glutamate quanta. The ganglion cell reencodes this information as brief bursts of one to six spikes separated by quiescent periods. When the stimulus is repeated, the number of spikes in a burst is highly reproducible (variance < mean) and spike timing is precise to within 10 ms, leading to an estimate that each spike encodes about 2 bits. To understand how the ganglion cell reencodes information, we studied the quantal patterns by repeating a white-noise stimulus and recording excitatory currents from a voltage-clamped, brisk-sustained ganglion cell. Quanta occurred in synchronous bursts of 3 to 65; the resulting postsynaptic currents summed to form excitatory postsynaptic currents (EPSCs). The number of quanta in an EPSC was only moderately reproducible (variance = mean), quantal timing was precise to within 14 ms, and each quantum encoded 0.1–0.4 bit. In conclusion, compared to a spike, a quantum has similar temporal precision, but is less reproducible and encodes less information. Summing multiple quanta into discrete EPSCs improves the reproducibility of the overall quantal pattern and contributes to the reproducibility of the spike train.

INTRODUCTION

Visual information from a natural scene causes a bipolar cell to continuously modulate its release of glutamate quanta. A ganglion cell receives these quanta, transforms them into brief inward currents, and reencodes them as a temporal pattern of spikes. This reencoding is little understood; this is in part because the stimulus used to measure quantal rates has been highly artificial: a near-saturating 1-s contrast that is much stronger and much longer than is common in nature. This stimulus evokes asynchronous release of as many as 45,000 quanta s^{-1} and sustained firing of <50 spikes s^{-1} (Freed 2000a,b). Taken uncritically, this would suggest that information from more than 900 quanta is reencoded as a single spike.

Recent studies of spike coding have used stimuli closer to natural by including a broad ensemble of temporal contrasts and frequencies. To such "white-noise" stimuli, a ganglion cell fires intermittently in brief bursts of one to six spikes (Berry et al. 1997; Koch et al. 2004), much as do lateral geniculate neurons to natural stimuli (Dan et al. 1996; Reinagel 2001). When the stimulus is repeated, the number of spikes in a burst is highly reproducible and a spike is timed accurately to within 10 ms, leading to the estimate that each spike encodes 1–3 bits (Koch et al. 2004; Passaglia and Troy 2004; Warland et al. 1997). This indicates a need to compare quantal release and spiking and raises some key questions regarding white-noise stimulation: *1*) how reproducible is quantal release?; *2*) how precisely timed are quanta?; *3*) what is the temporal structure of quantal release?; *4*) how many bits are encoded by one quantum?

To answer these questions, we presented white-noise stimuli to the intact retina while a small ganglion cell was voltage clamped to record glutamate currents. Quanta arrived at sufficiently high rates to overlap temporally, which obscured their individual arrival times. Thus, we analyzed their patterns indirectly by ensemble noise analysis (Sigworth 1981) and also calculated their information content (Shannon and Weaver 1963). We found that quanta arrive in bursts, much as spikes do, and that bursts sum into excitatory postsynaptic currents (EPSCs), although the release of a quantum is less reproducible than the firing of a spike. Thus summing many quanta into discrete EPSCs improves the reproducibility of the quantal pattern and contributes to the reproducibility of the spike train.

METHODS

Recording

From an adult Hartley guinea pig (400–600 g, >8 wk) anesthetized with ketamine (133 mg kg^{-1}), xylazine (13 mg kg^{-1}), and pentobarbital (100 mg kg^{-1}) an eye was removed and the animal was killed by anesthetic overdose. All procedures were performed in accordance with University of Pennsylvania and National Institutes of Health guidelines. Pieces of retina, attached to pigment epithelium, choroid, and sclera, were mounted in a chamber on an upright microscope with infrared differential interference contrast optics (Protti et al. 1997; Tian et al. 1998; Werblin 1978; Zhou 1998). The tissue was superfused with Ames' medium (Sigma, sigma.com) that was saturated with 5% CO_2-95% O_2, adjusted with glucose to about 300 mOsm, and which contained (in mM): 120 NaCl, 3.1 KCl, 0.5 KH_2PO_4, 23 Na_2HCO_3, 1.2 $MgSO_4$, 1.15 $CaCl_2$, plus amino acids and vitamins (pH 7.4, 34°C).

Patch electrodes (12 MΩ) were filled with (in mM): 110 Cs gluconate, 10 NaCl, 1 EGTA · 2.5 Na, 10 HEPES, 10 lidocaine *N*-ethyl bromide, 6 Lucifer Yellow, adjusted with glucose to 310 mOsm and with gluconate to pH 7.2 (Taylor and Vaney 2002). The calculated reversal potential for glutamate channels (E_{glut}), with equal permeability to Cs^+ and Na^+, was about 5 mV and the calculated reversal potential for Cl^- channels [γ-aminobutyric acid (GABA), glycine, E_{Cl^-}] was about −65 mV. All voltages were corrected for a calculated junction potential of −15 mV ($V_{mem} = -65 \rightarrow V_{hold} = -50$ mV). The recordings were acquired with an AxoPatch 200B patch-clamp amplifier (eight-pole Bessel filter, $f_c = 1$ kHz), and digitized online at 2 kHz using pClamp 7 (Axon Instruments, axon.com). Voltage-clamp recordings were performed in whole cell mode and were selected for a time constant (access resistance × cell capacitance) of <300 μs. Furthermore, cells with inadequate space clamp were rejected by examining their smallest EPSCs. The criterion for rejection was a significant negative correlation between peak

Address for reprint requests and other correspondence: M. A. Freed, 123 Anatomy–Chemistry Bldg., University of Pennsylvania School of Medicine, Philadelphia, PA 19104-6058 (E-mail: michael@retina.anatomy.upenn.edu).

The costs of publication of this article were defrayed in part by the payment of page charges. The article must therefore be hereby marked "*advertisement*" in accordance with 18 U.S.C. Section 1734 solely to indicate this fact.

amplitude and decay time constant. After recording, Lucifer-filled cells were photographed with a cooled-CCD camera (Hamamatsu, hamamatsu.com). The holding voltage was set at the Cl^- equilibrium potential to nullify inhibitory postsynaptic currents (IPSCs). Contamination by IPSCs was insignificant because all PSCs were blocked by the glutamate receptor antagonists 100 μM D(−)-2-amino-5-phosphonopentanoic acid and 10 μM 1,2,3,4-tetrahydro-6-nitro-2,3-dioxobenzo[f]quinoxaline-7-sulfonamide.

A light-emitting diode evenly illuminated the preparation (560 nm). A digital-to-analog converter provided voltages to a circuit that linearized diode intensity ($R^2 = 0.99$ for linear regression between voltage and intensity) and that provided rapid intensity changes with a time constant of 0.14 ms [$1/(2\pi\tau) > 1$ kHz]. Stimulus intensity was drawn at random from a Gaussian distribution at 1 kHz then low-pass filtered (100 Hz, four-pole). Recordings were acquired at 2 kHz using Clampex (Axon Instruments, axon.com) and analyzed off-line using IGOR (Wavemetrics, wavemetrics.com). For the information estimates only, to conserve analysis time, recordings were downsampled to 1 kHz (one-pole digital filter, $f_c = 500$ kHz).

Ensemble noise analysis of EPSCs

Consider an ensemble of EPSCs, each with charge Q which is the linear sum of n quanta where n has the Poisson probability distribution P(n) (Freed 2000a,b). The quantal charge has a Gaussian distribution with mean $\langle q \rangle$ and variance σ_q^2. Thus for all EPSCs composed on n quanta, Q is the sum of n random Gaussian-distributed variables and therefore has a Gaussian probability distribution with average $n\langle q \rangle$ and variance $n\sigma_q^2$, denoted G(Q, $n\langle q \rangle$, $n\sigma_q^2$). For all EPSCs composed on any number of quanta, the distribution of their charge Q is the sum a series of such Gaussian distributions, each weighted by its Poisson probability

$$p(Q) = \sum_n P(n)\mathrm{G}(Q, n\langle q \rangle, n\sigma_q^2) \tag{1a}$$

The average EPSC charge $\langle Q \rangle$ is by definition $\Sigma_Q\, Qp(Q)$ and thus

$$\langle Q \rangle = \sum_Q Q \sum_n P(n)\mathrm{G}(Q, n\langle q \rangle, n\sigma_q^2) \tag{1b}$$

Because $\Sigma_Q\, Q\mathrm{G}(Q, n\langle q \rangle, n\sigma_q^2)$ is by definition the average of the Gaussian distribution, which is $n\langle q \rangle$

$$\langle Q \rangle = \sum_n P(n) n\langle q \rangle \tag{1c}$$

Because $\Sigma_n\, P(n)n$ is by definition $\langle n \rangle$

$$\langle Q \rangle = \langle n \rangle \langle q \rangle \tag{1d}$$

The variance of an EPSC's charge is by definition

$$\sigma_Q^2 = \sum_Q (Q - \langle Q \rangle)^2 p(Q) \tag{2a}$$

$$\sigma_Q^2 = \sum_Q Q^2 p(Q) - 2\langle Q \rangle \sum_Q Qp(Q) + \langle Q \rangle^2 \sum_Q p(Q) \tag{2b}$$

Because $\Sigma_Q\, Qp(Q) = \langle Q \rangle$, because $\Sigma_Q\, p(Q) = 1$, and by *Eq. 1d*

$$\sigma_Q^2 = \sum_Q Q^2 p(Q) - \langle n \rangle^2 \langle q \rangle^2 \tag{2c}$$

Substituting *Eq. 1a* results in

$$\sigma_Q^2 = \sum_n Q^2 P(n)\mathrm{G}(Q, n\langle q \rangle, n\sigma_q^2) - \langle n \rangle^2 \langle q \rangle^2 \tag{2d}$$

Because $\Sigma_Q\, Q^2\mathrm{G}(Q, n\langle q \rangle, n\sigma_q^2)$ is the mean square of the Gaussian, which is equal to its variance plus its average squared

$$\sigma_Q^2 = \sum_n P(n)(n\sigma_q^2 + n^2\langle q \rangle^2) - \langle n \rangle^2 \langle q \rangle^2 \tag{2e}$$

$$\sigma_Q^2 = \sigma_q^2 \sum_n nP(n) + \langle q \rangle^2 \sum_n n^2 P(n) - \langle n \rangle^2 \langle q \rangle^2 \tag{2f}$$

Because $\Sigma_n\, nP(n) - \langle n \rangle$ and $\Sigma_n\, n^2P(n)$ is the mean square of the Poisson distribution, which is equal to its variance plus its average squared

$$\sigma_Q^2 = \sigma_q^2\langle n \rangle + \langle q \rangle^2(\sigma_n^2 + \langle n \rangle^2) - \langle n \rangle^2 \langle q \rangle^2 \tag{2g}$$

Because σ_n^2, the variance of the Poisson distribution, is equal to its mean

$$\sigma_Q^2 = \langle n \rangle(\sigma_q^2 + \langle n \rangle \langle q \rangle^2) \tag{2h}$$

Because the square of the coefficient of variation CV_q^2 is equal to $\sigma_q^2/\langle q \rangle^2$

$$\sigma_Q^2 = \langle n \rangle \langle q \rangle^2 [CV_q^2 + 1] \tag{3}$$

From *Eq. 1d* $\langle Q \rangle = \langle n \rangle \langle q \rangle$, therefore

$$\sigma_Q^2 = \langle Q \rangle \langle q \rangle [CV_q^2 + 1] \tag{4}$$

which can be rearranged to calculate the average quantal charge $\langle q \rangle$ (*Eq. 9,* RESULTS).

Noise sources

Ensemble analysis requires that noise be predominantly from bipolar cell synapses on the ganglion cell; thus the magnitude of other noise sources was considered. Virtually all instrument noise in a whole cell recording results from an access resistance R_a in conjunction with a cell membrane capacitance C_m. Instrument noise averaged 7×10^{-4} pA^2 across cells ($R_a = 35 \pm 8$ MΩ, $C_m = 27 \pm 6$ pF, *Eq. 16* of Sherman-Gold 1993), which when compared to total biological noise, calculated as the average difference between mean response and responses to stimulus repetitions, is insignificant (118 pA^2). A previous detailed analysis shows that photon noise, at the high absorption rates encountered during photopic illumination, is insignificant as is noise from presynaptic neurons and their synapses (Freed 2000a). Voltage-gated channel noise was made stationary by voltage clamp and contributed to variation in quantal charge q. Ensemble analysis corrected for this variation by including CV_q. Noise from amacrine synapses was excluded by recording at the Nernst potential of CL^-.

For ensemble analysis we selected the most stable recording to avoid inflating variance σ_Q^2, which might inflate $\sigma_Q^2/\langle Q \rangle$, and consequently the estimate quantal charge $\langle q \rangle$. To gauge recording stability, we measured this ratio averaged over consecutive quarters of an experiment and for the entire experiment and found no significant difference; thus the selected recording were sufficiently stable (367 ± 151 vs. 428 ± 187 pA · ms, *t*-test for paired variables, $P = 0.1$)

Deconvolution method of deriving temporal jitter

To derive the temporal jitter of a single quanta across stimulus repetitions, we first computed the shuffled crosscorrelation function S(t) between excitatory currents for different stimulus repetitions (Poisson predictor) (Ghose et al. 1994; Perkel et al. 1967). We then considered that S(t) has two components: *1*) the autocorrelation function for a single repetition represents correlations between the times of quanta convolved with correlations attributed to the time course of single quanta (Van der Kloot 1988); *2*) the jitter function J(t) represents the correlation between the times of quanta across different repetitions. Thus $S(t)$ is the convolution $A(t) * J(t)$. Accordingly we derived J(t) by deconvolving S(t) with A(t) (Koch et al. 2004).

Estimation of information rates

For the upper bound calculation, the signal was the response averaged across stimulus repeats $r(t)_{\text{avg}}$ and noise was the difference between the individual responses to stimulus repeats $r(t)_i$ and the average response (Borst and Theunissen 1999). The power spectrum of the signal-to-noise ratio was corrected for a finite number of stimulus repeats ($i = 1 \ldots m$) because a finite number would allow some noise to be measured as signal (van Hateren and Snippe 2001)

$$|SNR_{UB}(f)|^2 = \frac{m-1}{m}\frac{|R_{avg}(f)|^2}{\langle |R_{avg}(f) - R_i(f)|^2\rangle} - \frac{1}{m} \quad (5)$$

where capital letters denote the Fourier transform of a function and $\langle \ldots \rangle$ denotes averaging across a series of overlapping 1.024-s windows and then across stimulus repetitions.

Convolving a reverse filter with the response to a single stimulus presentation formed a reconstruction of the stimulus $s(t)_i^{est}$. The reverse filter was calculated for 5-s windows (zero-padded for fast Fourier transform) incremented by 1 s and was the cross-correlation of response $r(t)$ and stimulus $s(t)$ divided by the autocorrelation of the response

$$g(t) = \text{InverseFourier}\left[\frac{\langle R^*(f)S(f)\rangle}{\langle S^*(f)S(f)\rangle}\right] \quad (6)$$

where "*" denotes the complex conjugate.

For the lower bound calculation, the signal was the reconstruction and the noise was the difference between the reconstruction and the stimulus

$$|SNR_{LB}(f)|^2 = \frac{\langle |S_i^{\text{est}}(f)|^2}{\langle |S_i^{\text{est}}(f) - S(f)|^2\rangle} \quad (7)$$

The power spectra of the reconstruction and of the noise were both averaged across 1.024-s windows and repeats. As a control, from several long recordings (>50 stimulus repetitions) we used even repetitions to calculate the reverse filter and odd repetitions to make reconstructions. The resulting lower bounds were within one-half bit of the bounds calculated using the entire recording for both filter and reconstruction; thus in general we used the entire recording.

The upper limit for integrating information density was set for each cell by estimating its high-frequency cutoff. The cutoff was estimated by calculating the variance of $|\text{SNR}_{UB}|^2$ by delete-one resampling, then calculating 95% confidence limits (jackknife estimate of variance) (Borst and Theunissen 1999; Thomson and Chave 1991). The frequency at which the lower confidence limit crossed zero was taken as the cutoff frequency.

The upper bound estimate requires that noise, $r(t)_i - r(t)_{avg}$, has Fourier coefficients with independent, Gaussian distributions. Signal's departure from this requirement is allowed because it inflates information rate and is therefore consistent with an upper bound (Borst and Theunissen 1999; Rieke et al. 1997). To assess requirements of noise, we calculated Fourier coefficients for each overlapping 1.024-s window. We then constructed the probability distribution of Fourier coefficients as they varied across windows (converted to z-values, Fig. 1*A*). To access how close this distribution was to a Gaussian distribution, we calculated the distribution's entropy and found that it was smaller than the entropy of a Gaussian distribution with the same variance by only 1.0 ± 1.2% (averaged across cells; bin width for both distributions: 0.0001z). This small divergence from a Gaussian introduced an even smaller and negligible percent increase in the upper bound estimate (Rieke et al. 1997). We also calculated a correlation coefficient between the distribution at each frequency and at every other frequency (Pearson's *R*), confining correlations to those within a stimulus repetition. We found that 4.8 ± 2.5% of correlations had a 5% or greater probability of having zero correlation (Fisher's transformation of *R* to z-scores), as expected for independent distributions. Stimulus and noise were also virtually uncorrelated: the peak of their correlation function was typically 50 times smaller than the peak of the correlation between stimulus and response (Haag and Borst 1998).

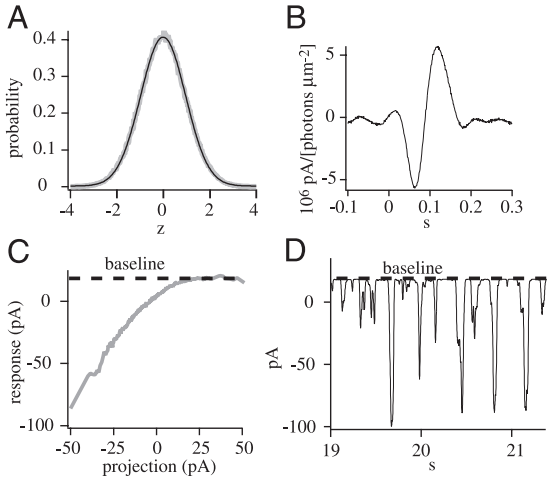

FIG. 1. Methods for characterizing quantal encoding of information. *A*: testing the assumption, for purposes of the upper bound information estimate, that noise has Fourier coefficients whose distribution across 1.024-s windows is Gaussian. At each frequency, we divided real and imaginary coefficients by the SD of their respective distributions to give z-scores, and then constructed the probability distribution of these scores for all frequencies and windows combined. Distribution, shown here for a typical cell (gray line), was well fit by a Gaussian function (dark line). *B*: finding the baseline current to estimate quantal rate. First step was to convolve a forward filter (shown here) with the stimulus to construct a projection of light intensity. *C*: second step to finding a baseline current was to construct a parametric plot of response and projection (shown here with both means subtracted). Near zero on the abscissa, corresponding to the mean stimulus intensity, the plot asymptoted to a baseline. *D*: when the baseline was superimposed on the average current, it matched the baselines of individual excitatory postsynaptic currents (EPSCs).

The lower bound estimate requires that signal has a Gaussian distribution: noise's divergence from a Gaussian contributes to an underestimate and is therefore consistent with a lower bound (Borst and Theunissen 1999). This requirement was met by using a Gaussian-distributed white-noise stimulus that, when convolved with a linear filter, ensured a Gaussian-distributed reconstruction.

Estimation of baseline current

To estimate quantal rate from excitatory currents required derivation of a baseline current corresponding to zero quantal rate. For a static stimulus, it would have been appropriate to estimate the baseline by graphing the response current against light intensity and finding where this current asymptotes at low intensities. For the dynamic stimulus used here, however, the response was graphed against a *projection* of the light intensity onto current ("static nonlinearity") (Chichilnisky 2001; Kim and Rieke 2001). The projection was constructed by calculating a forward filter as

$$f(t) = \text{InverseFourier}\left[\frac{\langle S^*(f)R(f)\rangle}{\langle R^*(f)R(f)\rangle}\right] \quad (8)$$

and then convolving the filter with the stimulus (Fig. 1*B*). The response was graphed against the intensity projection; its asymptote at low intensities was taken as the baseline (Fig. 1, *C* and *D*).

RESULTS

Eight ON brisk-sustained cells, known to have X-type receptive fields, were identified by their bushy dendrites that stratified diffusely in the ON stratum of the inner plexiform layer

(Boycott and Wässle 1974; Saito 1983; Stanford and Sherman 1984) (Fig. 2*A*). To isolate EPSCs caused by glutamate from bipolar cell ribbon synapses, the ganglion cell was voltage clamped in the whole cell mode at the reversal potential for chloride, thus nullifying inhibitory input. We presented a spatially uniform white-noise stimulus whose intensities had a Gaussian distribution with a mean of 2×10^5 photons μm^{-2} s^{-1} (photopic). Contrast, expressed as the SD of the Gaussian distribution, was one-fifth of the mean (Fig. 2*B*). The stimulus sequence lasted 25 s and was repeated 30–50 times. All frequencies were represented with equal power up to 100 Hz, which was above the cell's cutoff frequency (50 Hz; see below). The response to repeated presentations of the white-noise stimulus was a train of EPSCs reproduced with some variation across stimulus repetitions (Fig. 2*C*).

Reproducibility of quantal release

To characterize the reproducibility of quantal release, we tracked the charge transfer associated with an EPSC as it varied across stimulus repetitions. First we averaged the excitatory currents across stimulus repetitions; within this average we detected events with an amplitude above the noise (3 pA) and a decay phase well fit by an exponential ($R^2 > 0.7$, Fig. 3*A*)

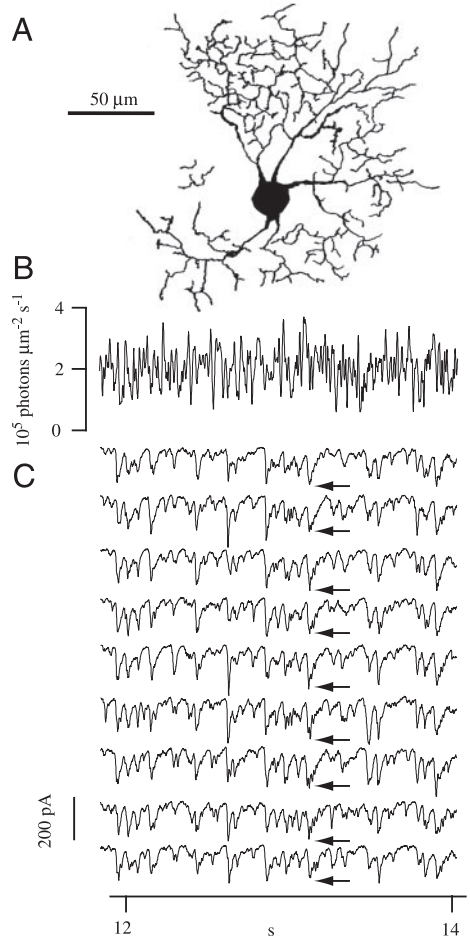

FIG. 2. Repeated white-noise stimulus evokes reproducible EPSCs. *A*: an ON brisk-sustained cell. *B*: 2-s portion of a 25-s-long flickering stimulus. *C*: whole cell recording of excitatory currents. EPSCs arising from bursts of quanta reproduced across stimulus repetitions (example EPSC indicated by arrows).

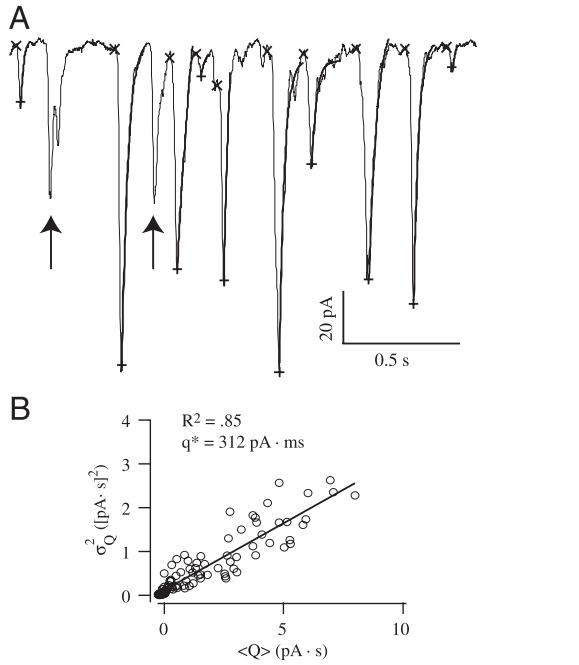

FIG. 3. Quanta follow Poisson statistics. *A*: EPSCs were identified by their leading edge (×), peak (+), and a decay well fit by a single exponential (—). Ensemble analysis requires synchronized quanta (see METHODS): thus 2 EPSCs (arrows) were rejected because they had decay phases with discontinuities. *B*: for each EPSC from the same cell as in *A*, the charge variance σ_Q^2 is graphed against mean charge $\langle Q \rangle$. Each point represents an EPSC. Variance and mean were proportional, consistent with Poisson release.

(Freed et al. 2003). The beginning of each EPSC was identified as a departure from baseline and the ending as a return to baseline. The detected EPSCs had a peak amplitude of 36 ± 8 pA, a rise time of 17 ± 3 ms, and a decay time constant of 237 ± 104 ms. Then for each stimulus repetition, the charge of an EPSC was calculated by integrating current between beginning and end. When the charge variance was graphed against its average, the data points were well fit by a line, indicating that variance was proportional to mean ($R^2 = 0.84 \pm 0.07$, Fig. 3*B*). This implied that the mean number of quantum composing an EPSC was equal to the variance of this number, consistent with quantal release following Poisson statistics.

Temporal precision of quantal release

To estimate timing precision of quantal release, we found the peak of each EPSC and measured its temporal deviations across repetitions (Fig. 4*A*). The distribution of temporal deviations was dome shaped and well fit by a Gaussian function (Fig. 4*B*). Temporal jitter, taken as the SD of this function, ranged from 6 to 13 ms and averaged 9 ± 3 ms. We also constructed the derivative of each EPSC, and found that the temporal jitter of its peak was not significantly different from the temporal jitter of the original EPSC (11 ± 4 ms, *t*-test for paired variables, 11 cells, $P > 0.1$).

Because this estimate was selective for multiquantal EPSCs that were consistently evoked across stimulus repetitions, we used an additional deconvolution method of estimating temporal jitter (METHODS) (Koch et al. 2004). This resulted in a dome-shaped distribution well fit with a Gaussian function. The temporal jitter, the SD of this function, ranged from 5 to 14 ms and averaged 8 ± 3 ms (Fig. 4*C*). The temporal jitters

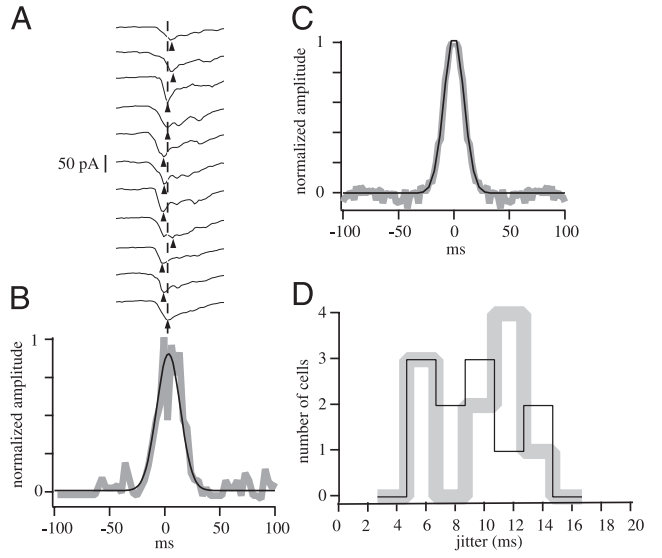

FIG. 4. Temporal precision of quantal release. *A*: negative peak of an EPSC (arrowheads) shows temporal deviations from the dashed line. *B*: distribution of temporal deviations for EPSCs in one recording (50 EPSCs, 10 stimulus repetitions). Temporal jitter, equal to the SD of Gaussian fit, was 11 ms. *C*: distribution of temporal deviations estimated by deconvolution method (same recording as in *B*). Temporal jitter from Gaussian fit was 9 ms. *D*: distribution of temporal jitter across 11 brisk-sustained cells measured from EPSCs (gray line) and by deconvolution (black line).

estimated from EPSCs or by deconvolution were not significantly different from one another (Fig. 4*D,* 11 cells, $P > 0.3$).

Charge associated with a single quantum

The charge transfer associated with a single quantum was estimated by ensemble analysis of EPSCs (Sigworth 1981). Quantal charge was calculated as (see METHODS)

$$q^* = \frac{\sigma_Q^2}{\langle Q \rangle}[CV_q^2 + 1]^{-1} \quad (9)$$

where Q is the EPSC's charge, and $\langle Q \rangle$ and σ_Q^2 are its mean and variance. The quantity CV_q, the quantal charge's coefficient of variation, was measured directly from the smallest EPSCs to be 1.8 ± 0.3 (see below). The ratio σ_Q^2/Q, taken from the slope of the regression fit (Fig. 3*B*), was 340 ± 90 pA · ms, and the resulting quantal charge was 70 ± 44 pA · ms.

The estimated quantal charge can be compared to those of quanta recorded in other ganglion cells. Because the quantal charge will vary with the holding voltage or resting potential, we converted it to an integral of conductance. This integral was calculated as $\int g(t)dt = q^*/(E_{glut} - E_{hold})$ (Freed 2000b), which for an E_{glut} of 5 mV and an E_{hold} of −65 mV, was equal to 1,000 pS · ms. Spontaneous EPSCs in other mammalian ganglion cells have a peak conductance of 100 pS, a decay time constant of 1–6 ms (Protti et al. 1997; Tian et al. 1998), and therefore a conductance integral (peak conductance × time constant) of about 100–600 pS · ms. Light-evoked quanta from the brisk-sustained cell of cat retina also exhibits a similar quantal conductance integral (100–800 pS · ms) (Freed 2000a). Thus quanta recorded here are similar to quanta from other ganglion cells.

Estimate of error in ensemble analysis

Our method of ensemble analysis selected EPSCs composed of synchronized quanta to ensure that quanta are complete within the time limits over which each EPSC was integrated to derive charge. We wondered whether these quanta were part of the same charge distribution as unsynchronized quanta. To test this idea and to estimate the error of ensemble analysis we compared the estimated charge for a quantum to the charge measured for the smallest EPSCs. We identified these smallest EPSCs in responses to single stimulus presentations by making the criterion fit to the decaying phase more stringent than for large EPSCs ($R^2 > 0.9$, Fig. 5*A*). The detected EPSCs had peak amplitudes of 12 ± 5 pA, indicating a peak conductance of about 170 pS, a rise time of 1.8 ± 0.7 ms, and a decay time constant of 18 ± 8 ms ($E_{glut} = 5$ mV, $E_{memb} = -65$ mV). Their average charge was 69 ± 38 pA · ms, which was very close to the quantal charge estimated by ensemble analysis (70 ± 44 pA · ms).

The quantal charge q^* estimated from ensemble analysis varied somewhat from cell to cell. If this analysis was accurate, then the estimate q^* should vary commensurately with the charge measured for the smallest EPSCs q'. To check this, q^* was graphed against q'. The resulting data points fell on either side of the diagonal line $q^* = q'$, indicating that the smallest EPSCs are composed of approximately one quantum, and indicating that unsynchronized quanta and those synchronized into EPSCs convey similar charge (Fig. 5*B*). From this graph, a brief calculation was made of error. If all error was in the estimate q^* and *none* in the measure q' then the error for q^* would be $\sqrt{\Sigma(q^*-q')^2/N}$, which equals about 35% of the mean value of q*. If, as was more likely, q* and q′ had approximately equal errors, then each would have an error of about $35\%/\sqrt{2} = 25\%$. This implied that the ensemble analysis estimated quantal charge reasonably well.

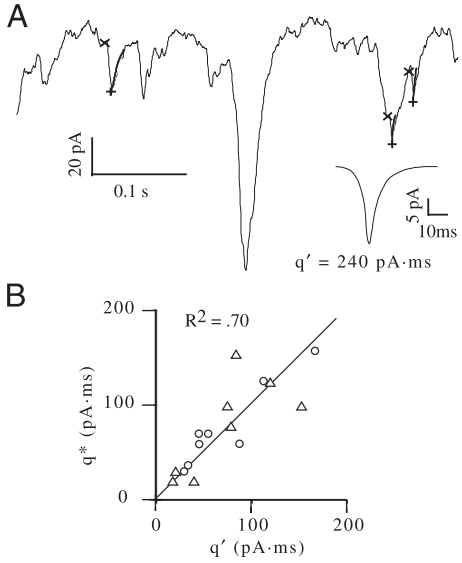

FIG. 5. Checking accuracy of ensemble analysis: *A*: smallest EPSCs from a single stimulus presentation. *Inset:* average of smallest EPSCs. *B*: quantal charge estimated by ensemble analysis (q^*) graphed against average charge of the smallest EPSCs (q'). Each point represents an ON brisk-sustained (△) or other ganglion cell (○) (16 cells). Points fall along the $q^* = q'$ line, indicating that estimate of quantal charge was accurate.

Temporal structure of quantal release

The white-noise stimulus contained a broad ensemble of intensities and frequencies, which evoked EPSCs of variable quantal content. To estimate quantal content, we waived the criterion that the decaying phase was well fit by an exponential in order to obtain a more representative sample (including those with imperfectly synchronized quanta). This increased the number of identified EPSCs by 22 ± 11%. We then divided an EPSC's charge Q by the estimated quantal charge q^* (Fig. 6*A*). Across EPSCs, quantal content exhibited a skewed distribution, with three quanta the most common value and 65 quanta near the largest (average quantal content = 19 ± 4 vesicles; Fig. 6*B*).

To estimate mean quantal rate across the ensemble of stimulus contrasts and frequencies, we first derived the baseline current corresponding to zero release rate (METHODS, Fig. 1). Then to calculate current arising from quantal release (continuous current) we subtracted this baseline from the time-averaged current. Finally, to calculate quantal rate we divided continuous current by the quantal charge q^*. Across cells the continuous current averaged 10 ± 5 pA, which gave a mean quantal rate of 112 ± 19 quanta s^{-1} (see METHODS, Fig. 6*C*).

Quantal rate at a single synapse is modest

These data allow an estimate of quantal rate at a single synapse. Although the exact number of synapses on the brisk-sustained cell of guinea pig is not known, its dendritic field is similar in size to that of a peripheral ganglion cell in the cat retina, which has about 2,000 ribbon synapses (Freed 2000a; Kier et al. 1995). Thus a quantal rate of 112 s^{-1} would suggest about 0.06 quanta s^{-1} at each synapse. This is quite modest when compared with the maximal sustained rate for a bipolar cell ribbon synapse of about 40 s^{-1} (Freed 2000a,b).

It is also possible to estimate the average number of quanta contributed by each synapse to an EPSC. The largest EPSCs composed of 65 quanta would require about 3% of synapses to release a quantum. Even if the number of synapses is overestimated by an order of magnitude—indicating 0.6 quanta s^{-1} and 30% of synapses releasing a quantum— the present data clearly indicate that during white-noise stimulation, a synapse uses only a fraction of its capacity to release vesicles.

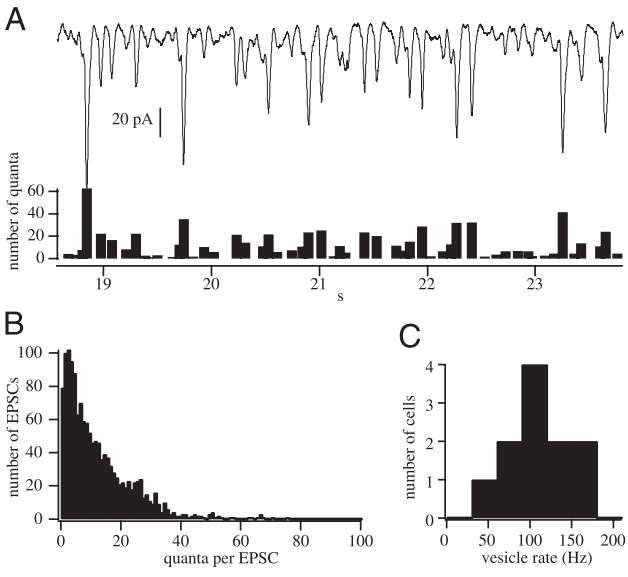

FIG. 6. Temporal structure of quantal release. *A*: quantal content of EPSCs identified in averaged excitatory current. *B*: distribution of quantal content across EPSCs from 7 ON brisk-sustained cells. *C*: distribution of average vesicular release rates (11 recordings from 8 ON brisk-sustained cells).

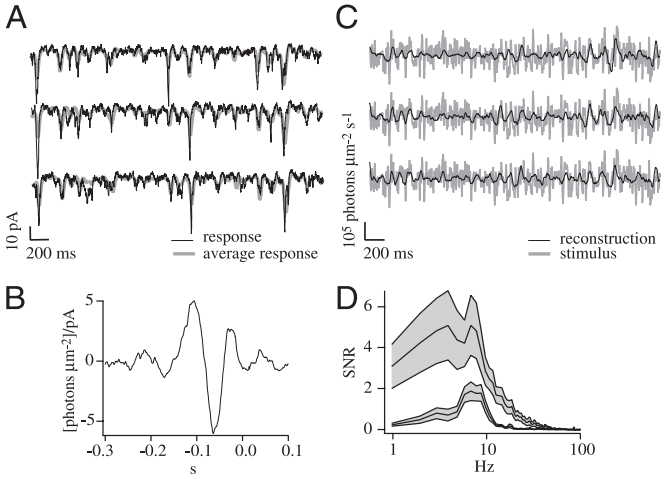

FIG. 7. Measuring signal-to-noise ratio for upper and lower bounds on information. *A*: for the upper bound estimate, signal was the excitatory current averaged across stimulus repetitions—the average response—and noise was the response to each stimulus repetition minus the average response. *B*: typical reverse filter. Filter was convolved with the response to each stimulus presentation to produce a reconstruction. *C*: for the lower bound estimate, signal was the stimulus and noise was each individual reconstruction minus the stimulus. *D*: power spectra of signal-to-noise ratio for upper and lower bounds including 95% confidence limits. Averaged across 8 ON brisk-sustained cells.

Information rate

To set bounds on information rate, the power spectrum of the signal-to-noise ratio was first calculated (METHODS). For the upper bound, signal was the excitatory current averaged across stimulus repetitions and noise was the difference between the average and the excitatory current from each stimulus presentation (Fig. 7*A*). For the lower bound, a reconstruction of the stimulus was made from each excitatory current (Fig. 7*B*); signal was the stimulus and noise was the difference between the stimulus and each reconstruction (Fig. 7*C*). The resulting signal-to-noise ratio spectra peaked at around 8 Hz (Fig. 7*D*), similar to the frequency of peak contrast sensitivity of the ON brisk-sustained spike train in the cat retina (~10 Hz) (Frishman et al. 1987).

Information density was calculated by plugging the signal-to-noise spectra into Shannon's equation (METHODS) (Bialek et al. 1991; Borst and Theunissen 1999; Warland et al. 1997). Integrating information density between zero and the signal's high-frequency cutoff (50 ± 23 Hz) resulted in an upper bound of 53 ± 22 bits s^{-1} and a lower bound of 13 ± 3 bits s^{-1} (Fig 8*A*).

A quantum encodes less than one bit

To estimate information per quantum, the bounds on information rate for a cell were divided by its average quantal rate. This gave for all cells 0.11 ± 0.02 to 0.43 ± 0.08 bits per quantum. Because a lengthy stable recording (~0.5 h) was needed to estimate information, the effect of different stimulus

contrasts on quantal information content was not systematically tested. However, for three ON brisk-sustained cells, an additional stimulus with the same mean intensity as the standard one, but half the modulation was presented. For this lower modulation both quantal rates and information rates were lower (Table 1). Temporal jitter and the mean number of quanta in an EPSC were not significantly different (*t*-test, $P > 0.7$). Finally, the bounds on information encoded by a single quantum were not significantly different, indicating that a quantum consistently encodes less than a bit of information (Table 1).

If the information conveyed by a quantum were constant, then information rate would be proportional to quantal rate as it varied across cells and across stimulus contrasts. This appeared to be true because when either the upper or lower bound on information was graphed against quantal rate, a line adequately fit the data points (Fig. 8*B*).

TABLE 1. *Information transmission by quantal release*

Stimulus Modulation	Quantal* Rate, s^{-1}	Information* Rate, bits s^{-1}	Information per quantum, bits
1/10 of mean	56 ± 26	11 ± 4–30 ± 12	0.12 ± 0.03–0.44 ± 0.20
1/5 of mean	112 ± 19	13 ± 3–52 ± 22	0.11 ± 0.02–0.43 ± 0.08

Statistically significant difference: * $P < 0.01$.

DISCUSSION

We can now compare quantal release to spiking as described for brisk ganglion cells under conditions very similar to those used here (in vitro preparation of intact guinea pig retina, white-noise stimulation, SD one-third of mean) (Berry et al. 1997; Koch et al. 2004). First, quantal release is less reproducible than spiking because variance of quanta in a burst is equal to the mean but the variance of spikes in a burst is substantially less than the mean (Berry et al. 1997; van Steveninck et al. 1997). The temporal jitter of quantal release, 5–12 ms, substantially overlaps that of spiking (1–10 ms) (Berry et al. 1997; Koch et al. 2004). The number of quanta in a burst EPSC is composed of 3–65 quanta, much more than the number of spikes in a burst (1–6) (Berry et al. 1997; Koch et al. 2004). Average quantal rate is on the order of 100 s^{-1}, much more than spike rate (about 10 s^{-1}) (Berry et al. 1997; Koch et al. 2004). This indicates roughly 10 quanta trigger a spike, much less than the 900 suggested by responses to artificially sustained high contrasts (see INTRODUCTION) (Freed 2000a,b). A quantum encodes 0.1–0.4 bit, much less than a spike's 2 bits (Berry et al. 1997; Koch et al. 2004). This indicates it takes 5–20 quanta to encode as much information as a spike, consistent with about 10 quanta to trigger a spike. Thus the overall temporal patterns of quanta and spikes are similar because they occur in bursts and have similar temporal precision, but a quantum is less reproducible and encodes less information.

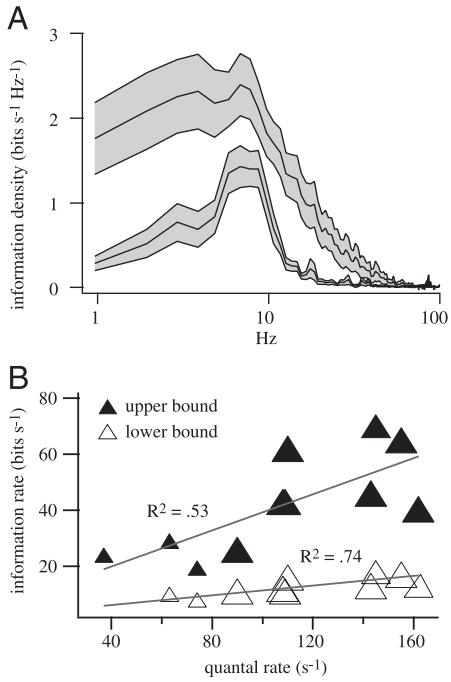

FIG. 8. A quantum encodes less than 1 bit. *A*: upper and lower bounds for information density calculated by substituting power spectra into *Eqs. 5* and *7*, respectively. Bounds for information rate were calculated by integrating information density from 0 to 50 Hz (see METHODS). *B*: graph of information rate against quantal rate. Each point represents an ON brisk-sustained cell except 3 cells were presented with 2 different stimulus modulations. Modulation, expressed as SD of Gaussian distribution, was either 1/5th (large symbols) or 1/10th of mean (small symbols). Slopes of 2 regression lines set bounds on the information per quantum: 0.1 and 0.4 bits, respectively.

Functional implications

The most salient feature of quantal release during white-noise stimulation is its burstiness. Presumably bursts occur when a cell encounters its "favorites" from an ensemble of temporal patterns (Keat et al. 2001). Thus it has been suggested that burst timing encodes *when* a pattern occurs, and burst size encodes *how much* of this pattern is present (Keat et al. 2001). However, bursts also aid in the reencoding of information from quanta to spikes. Consider that quanta occur in average bursts of $n = 20$. According to Poisson statistics, the signal is n, the noise is $\sqrt{n}$, and thus the signal-to-noise ratio is about 4.5. If release were asynchronous and still Poisson, however, the number of quanta in an integration time would determine the signal-to-noise ratio. For an average quantal rate of 100 s^{-1} there would be only about $n = 2$ quanta in an integration time equal to the quantal decay time constant (~20 ms) and thus a signal-to-noise ratio of only 1.4. Thus bursts increase signal-to-noise ratio and enhance reproducibility of the overall quantal pattern, and consequently enhance reproducibility of the resulting spike pattern.

The reproducibility of spike trains is also enhanced by a refractory period that regularizes spike rate (Berry and Meister 1998; Kara et al. 2000). Consistent with this idea, the distribution of interspike intervals is well fit by a gamma function, which is the interval distribution that results from a Poisson process with the shortest intervals removed (Troy and Robson 1992). Quantal release apparently does not benefit from such a refractory period because, although the release from a single ribbon synapse may briefly inhibit subsequent release (DeVries 2001; Palmer et al. 2003), multiple synapses can release quanta simultaneously.

Although the information rate and quantal rate varied with contrast and across cells, a single quantum fairly consistently encodes 0.1–0.4 bit. This seems like a small amount of information. Even a simple binary code, which relies on the presence or absence of an event, can encode at least one bit per

event. A spike does even better than this: across a variety of neural systems it can almost universally encode 1–3 bit (Fairhall et al. 2001; Reinagel and Reid 2000; Rieke et al. 1997; Theunissen et al. 1996). A spike's encoding capacity is high because the spike rate is low and because intervals of time without a spike convey as much information as those that contain a spike (Rieke et al. 1997).

Apparently if quantal rate were reduced to match spike rate and a refractory period was introduced, the coding capacity of a quantum would approach the coding capacity of a spike (Rieke et al. 1997). Although this may seem fantastic, such a stratagem may be followed by some small neurons. A cerebellar granule cell receives only intermittent quanta from a few mossy fiber rosettes. An auditory afferent receives input from a single hair cell. These cells' high input resistances (1 GΩ vs. 50 MΩ for the ON brisk-sustained cell) allow each quantum to trigger a spike (Carter and Regehr 2002; Chadderton et al. 2004). Thus for these cells, quantum and spike may both achieve more than one bit.

Why then, if very low rates increase information per event, does a ganglion cell receive quanta at the moderate rate that it does? First, the ganglion cell integrates convergent information from many cones, which presumably absolutely requires sufficient quantal rates to encode sufficient information rates. Second, signaling by glutamatergic neurons uses up a substantial portion (~50%) of the total energy requirements of the retina, thus exactly how energy is expended on information encoding matters greatly (Ames and Li 1992). Nevertheless, reencoding multiple quanta into a single spike may have only a small impact on the total energy expense. It has been estimated for a cortical pyramidal cell that a glutamate quantum requires 1,000-fold *fewer* ATP molecules than a spike (Attwell and Laughlin 2001). This suggests that the best strategy is to sum multiple quanta to improve the reproducibility of an EPSC, thus reducing the amount of noise imparted to the spike train, and increasing bits per spike. Because a quantum is much cheaper energetically than a spike, using many quanta to trigger a spike would add to the total energy cost of encoding information by only a small amount.

ACKNOWLEDGMENTS

Thanks to P. Sterling and C. Ratliff for valuable advice.

GRANTS

This work was supported by National Institutes of Health Grant EY-13333.

REFERENCES

Ames A and Li YY. Energy requirements of glutamatergic pathways in rabbit retina. *J Neurosci* 12: 4234–4242, 1992.

Attwell D and Laughlin SB. An energy budget for signaling in the grey matter of the brain. *J Cereb Blood Flow Metab* 21: 1133–1145, 2001.

Berry MJ and Meister M. Refractoriness and neural precision. *J Neurosci* 18: 2200–2211, 1998.

Berry MJ, Warland DK, and Meister M. The structure and precision of retinal spike trains. *Proc Natl Acad Sci USA* 94: 5411–5416, 1997.

Bialek W, Rieke F, de Ruyter van Steveninck RR, and Warland D. Reading a neural code. *Science* 252: 1854–1857, 1991.

Borst A and Theunissen FE. Information theory and neural coding. *Nat Neurosci* 2: 947–957, 1999.

Boycott BB and Wässle H. The morphological types of ganglion cells of the domestic cat's retina. *J Physiol* 240: 397–419, 1974.

Carter AG and Regehr WG. Quantal events shape cerebellar interneuron firing. *Nat Neurosci* 5: 1309–1318, 2002.

Chadderton P, Margrie TW, and Hausser M. Integration of quanta in cerebellar granule cells during sensory processing. *Nature* 428: 856–860, 2004.

Chichilnisky EJ. A simple white noise analysis of neuronal light responses. *Network* 12: 199–213, 2001.

Dan Y, Atick JJ, and Reid RC. Efficient coding of natural scenes in the lateral geniculate nucleus: experimental test of a computational theory. *J Neurosci* 16: 3351–3362, 1996.

DeVries SH. Exocytosed protons feedback to suppress the Ca^{2+} current in mammalian cone photoreceptors. *Neuron* 32: 1107–1117, 2001.

Fairhall AL, Lewen GD, Bialek W, and de Ruyter Van Steveninck RR. Efficiency and ambiguity in an adaptive neural code. *Nature* 412: 787–792, 2001.

Freed MA. Parallel cone bipolar pathways to a ganglion cell use different rates and amplitudes of quantal excitation. *J Neurosci* 20: 3956–3963, 2000a.

Freed MA. Rate of quantal excitation to a retinal ganglion cell evoked by sensory input. *J Neurophysiol* 83: 2956–2966, 2000b.

Freed MA, Smith RG, and Sterling P. Timing of quantal release from the retinal bipolar terminal is regulated by a feedback circuit. *Neuron* 38: 89–101, 2003.

Frishman LJ, Freeman AW, Troy JB, Shweitzer-Tong DE, and Enroth-Cugell C. Spatiotemporal frequency responses of cat retinal ganglion cells. *J Gen Physiol* 89: 599–627, 1987.

Ghose GM, Ohzawa I, and Freedman RD. Receptive-field maps of correlated discharge between pairs of neurons in the cat's visual cortex. *J Neurophysiol* 71: 330–346, 1994.

Haag J and Borst A. Active membrane properties and signal encoding in graded potential neurons. *J Neurosci* 18: 7972–7986, 1998.

Kara P, Reinagel P, and Reid RC. Low response variability in simultaneously recorded retinal, thalamic, and cortical neurons. *Neuron* 27: 635–646, 2000.

Keat J, Reinagel P, Reid RC, and Meister M. Predicting every spike: a model for the responses of visual neurons. *Neuron* 30: 803–817, 2001.

Kier CK, Buchsbaum G, and Sterling P. How retinal microcircuits scale for ganglion-cells of different size. *J Neurosci* 15: 7673–7683, 1995.

Kim KJ and Rieke F. Temporal contrast adaptation in the input and output signals of salamander retinal ganglion cells. *J Neurosci* 21: 287–299, 2001.

Koch K, McLean J, Berry M, Sterling P, Balasubramanian V, and Freed MA. Efficiency of information transmission by retinal ganglion cells. *Curr Biol* 14: 1523–1530, 2004.

Palmer MJ, Hull C, Vigh J, and von Gersdorff H. Synaptic cleft acidification and modulation of short-term depression by exocytosed protons in retinal bipolar cells. *J Neurosci* 23: 11332–11341, 2003.

Passaglia CL and Troy JB. Information transmission rates of cat retinal ganglion cells. *J Neurophysiol* 91: 1217–1229, 2004.

Perkel DH, Gerstein GL, and Moore GP. Neuronal spike trains and stochastic point processes. II. Simultaneous spike trains. *J Neurophysiol* 7: 419–440, 1967.

Protti DA, Gerschenfeld HM, and Llano I. GABAergic and glycinergic IPSCs in ganglion cells of rat retinal slices. *J Neurosci* 17: 6075–6085, 1997.

Reinagel P. How do visual neurons respond in the real world? *Curr Opin Neurobiol* 11: 437–442, 2001.

Reinagel P and Reid RC. Temporal coding of visual information in the thalamus. *J Neurosci* 20: 5392–5400, 2000.

Rieke F, Warland D, Steveninck RdRv, and Bialek W. *Spikes: Exploring the Neural Code.* Cambridge, MA: MIT Press, 1997.

Saito HA. Morphology of physiologically identified X-, Y-, and W-type retinal ganglion cells of the cat. *J Comp Neurol* 221: 279–288, 1983.

Shannon C and Weaver W. *Mathematical Theory of Communication.* Urbana, IL: Univ. of Illinois Press, 1963.

Sherman-Gold R. *The Axon Guide for Electrophysiology & Biophysics Laboratory Techniques.* Foster City, CA: Axon Instruments, 1993.

Sigworth FJ. Covariance of nonstationary sodium current fluctuations at the node of Ranvier. *Biophys J* 34: 111–133, 1981.

Stanford LR and Sherman SM. Structure/function relationships of retinal ganglion cells in the cat. *Brain Res* 297: 381–386, 1984.

Taylor WR and Vaney DI. Diverse synaptic mechanisms generate direction selectivity in the rabbit retina. *J Neurosci* 22: 7712–7720, 2002.

Theunissen F, Roddey JC, Stufflebeam S, Clague H, and Miller JP. Information theoretic analysis of dynamical encoding by four identified primary sensory interneurons in the cricket cercal system. *J Neurophysiol* 75: 1345–1364, 1996.

Thomson DJ and Chave AD. Advances in spectrum analysis and array processing. In: *Advances in Spectrum Analysis and Array Processing,* edited by Haykin S. Englewood Cliffs, NJ: Prentice Hall, 1991, p. 58–113.

Tian N, Hwang TN, and Copenhagen DR. Analysis of excitatory and inhibitory spontaneous synaptic activity in mouse retinal ganglion cells. *J Neurophysiol* 80: 1327–1340, 1998.

Troy JB and Robson JG. Steady discharges of X-Retinal and Y-Retinal ganglion cells of cat under photopic illuminance. *Vis Neurosci* 9: 535–553, 1992.

Van der Kloot W. Estimating the timing of quantal releases during end-plate currents at the frog neuromuscular junction. *J Physiol* 402: 595–603, 1988.

van Hateren JH and Snippe HP. Information theoretical evaluation of parametric models of gain control in blowfly photoreceptor cells. *Vision Res* 41: 1851–1865, 2001.

van Steveninck RRD, Lewen GD, Strong SP, Koberle R, and Bialek W. Reproducibility and variability in neural spike trains. *Science* 275: 1805–1808, 1997.

Warland DK, Reinagel P, and Meister M. Decoding visual information from a population of retinal ganglion cells. *J Neurophysiol* 78: 2336–2350, 1997.

Werblin FS. Transmission along and between rods in the tiger salamander retina. *J Physiol* 280: 449–470, 1978.

Zhou ZJ. Direct participation of starburst amacrine cells in spontaneous rhythmic activities in the developing mammalian retina. *J Neurosci* 18: 4155–4165, 1998.